JOURNAL OF AIRCRAFT
Vol. 41, No. 6, November–December 2004

Level Estimation of Extended Acoustic Sources Using a Parametric Method

Daniel Blacodon* and Georges Élias†
ONERA/DSNA, 92322 Châtillon CEDEX, France

Array processing is a powerful tool to extract the noise source characteristics from the acoustic signals measured during wind-tunnels tests. For many years, this measurement technology is commonly being used to study airframe noise. Conventional beam forming methods have proven their efficiency in source localization, but it is well known that they are limited in the estimation of the power levels of extended sources. An approach based on a spectral estimation method (SEM) is proposed in order to determine the actual sound-pressure levels of the acoustic sources found by the localization method. The SEM is based on the array cross-spectral matrix, which contains an indirect measurement of the source power levels of interest and on a modeling of this matrix. Optimal estimates of the actual source power levels can be obtained by minimizing the mean square error between the measurement and model matrices. However, the direct minimization suffers from the sensitivity to noise inherent in the ill-posed nature of the problem. To obtain meaningful results, the problem is regularized by using a priori information. Numerical simulations involving multiple source areas are provided to illustrate the effectiveness of the estimation procedure. The method is successfully applied to compute the power levels of the main sources on a 1/11th-scaled model of the Airbus A320/A321 tested in CEPRA 19 wind tunnel.

Nomenclature

$C^{mes}_{m,n}(\tau)$	=	cross correlation between $p^{mes}_m(t)$ and $p^{mes}_n(t)$
$C^{mod}_{m,n}(\tau)$	=	cross correlation between $p^{mod}_m(t)$ and $p^{mod}_n(t)$
c	=	sound speed in the propagation medium
$\mathcal{D}$	=	region containing all of the acoustic source areas D_q
D_q	=	region containing the acoustic source distribution q
E	=	expectation operation
f	=	frequency, Hz
f_s	=	sampling frequency of the measurement signals, Hz
I	=	pitch angle
k	=	acoustic wave number
M	=	number of microphones in the array
$P_{I,q}$	=	integrated power levels of the source area q
$p^{mes}_n(t)$	=	nth microphone measurement signal
$p^{mod}_n(t)$	=	nth model signal
Q	=	total number of source areas in $\mathcal{D}$
T	=	total duration of the recorded signal, s
t	=	time, s
V	=	wind-tunnel flow velocity
(x_1, x_2)	=	plane containing both the acoustic source areas and the array
$[\Gamma^{mes}(f)]$	=	cross-spectral matrix resulting from the acoustic measurement
$[\Gamma^{mod}(f)]$	=	cross-spectral matrix obtained with the model
τ	=	time delay

I. Introduction

IN the classical multiple acoustic sources localization problem the sensor signals produced by the wave fields are processed in order to isolate the incident sources and estimate their associated positions. A wide variety of techniques has been developed to provide solutions to this problem. The acoustic mirror[1,2] technique uses a single microphone placed at one elliptic focal point. The characterization of an entire source region of interest is obtained by moving the mirror in order to focus on different regions on the source. With an array of microphones, signal processing by conventional beamforming (CBF) supplies a source map in a single step. The array itself can be linear,[3] cross shaped,[4,5] circular,[6,7] etc. Processing based on CBF is the optimum processing for a single monopole. The classical result is that the overall array response to a point source exhibits several sidelobes and a main lobe of which the location and amplitude correspond respectively to the location and amplitude of the point source.[4,8]

For multiple sources, the CBF method is able to perform the localization with a good degree of accuracy in many practical situations.[9,10] The power levels of the sources are accurately obtained when the sources are separated from each other by at least one 3-dB beam width and when their amplitudes are larger than the sidelobe ones. Unfortunately, the two preceding criteria are not satisfied in situations of interest like aircraft noise, when the sources under study are continuously distributed, and the beam pattern associated with different sources overlaps. In these cases, it is obvious that, because of its poor spatial resolution, the CBF method fails to provide correct levels.

The estimation of the source power levels in a multiple source environment is essential in order to characterize airframe noise. To solve the problem, we must resort to methods that improve the overall performance of the CBF. An interesting solution has been suggested by Brooks and Humphreys[11] for computing the total output of distributed sources. It consists in recovering the actual source power levels of specified areas from the CBF output, knowing the characteristics of the array pattern. In this study, the undesirable effects of smearing by the array pattern are removed from the output of the CBF by using an inverse function that takes the beam form into account. After this step, the total level output of a specified area is obtained after integration over this area. The method that has just been outlined can provide the source level with a good degree of accuracy. However, we must recall that this method is based on the data provided by the CBF. In practice, these data do not only contain the noise radiation from the source of interest, but also random noise, which always contaminates measurements. Generally, the background noise has a spectrum, which is more extended than

Presented as Paper 2003-3199 at the AIAA/CEAS 9th Aeroacoustics Conference and Exhibit, Hilton Head, SC, 12 May 2003; received 12 June 2003; revision received 18 May 2004; accepted for publication 30 May 2004.

*Research Engineer, Computational Fluid Dynamics and Aeroacoustics Department, BP 72; Daniel.Blacodon@onera.fr.

†Research Manager, Computational Fluid Dynamics and Aeroacoustics Department, BP 72; Georges.Elias@onera.fr.

the spectra of the source areas, and it can often become dominant as the frequency increases. Consequently, the particular solutions associated with background noise can be superposed to the solution of our problem in an unfavorable way by the normalization operation used to approximate the source power levels and lead to inaccurate results. It is shown in Ref. 11 that the undesirable contribution of background noise can be reduced by removing the main diagonal of the cross-power matrix before computing the CBF.

In this paper we propose a spectral estimation method (SEM)[12–14] to compute the power levels of the distribution of sources. This method is based on the cross-spectral matrix (CSM), which has the advantage of not being corrupted by the array response. Our purpose here is to obtain a method with high-resolution capabilities thanks to direct use of the CSM. In other words, the main lobe in the beam pattern of a point source is expected to be as narrow as possible and the height of the sidelobes as small as possible. The premise for the development of the method is based on the fact that the array CSM can be viewed as indirect measurement of the source power levels of interest. Because the measured CSM is known, the problem here is to model the sources and find the parameters (i.e., the power levels of the source areas) of a corresponding model matrix that respect the observed CSM. A standard approach in the estimation procedure consists of sampling the source area and considering that for each sampled source element there is a candidate monopole source whose power level remains to be found. A method for fitting the measured CSM to the model one is then implemented to determine the amplitudes of the point sources. However, the errors on the model and the effect of background noise on the measurements mean that the inverse transformation is not unique, that is, there are several solutions that yield the same output. One way to circumvent this difficulty (i.e., regularize the problem) is to include as much a priori information upon the input as possible. We will adopt this approach and, for instance, seek solutions with positive amplitudes.[15,16] Two classes of methods can solve the problem numerically. The direct methods belong to the first category. They are based on the inversion of a matrix, which is often ill conditioned. The second class is iterative methods, which do not have these drawbacks. It is however necessary to initiate them and find a criterion to stop the iterative process. The iterative method known as conjugated gradient has been chosen for this study for its numerical stability and fast convergence in a search space, which is not too extended thanks to the use of a priori information.

We begin with some considerations on a source area description and present the problem to solve in Sec. II. The array CSM and its modeling are discussed in Sec. III. The estimation of power levels of extended sources is examined in Sec. IV. Numerical simulations presented in Sec. V aim at comparing the spatial resolution between the CBF and the spectral estimation method (SEM) and to examine the accuracy of the SEM in complex situations. Section VI provides the noise source characterization results derived from the experiments.

II. Source Function and Estimation Problem

Before proceeding with a detailed discussion of the spectral estimation method that has been developed in this study to find the power levels of sound sources, it is important to clarify the notion of acoustic source and the nature of the problem we propose to solve.

A. How to Describe a Source Area

Let us consider, in the absence of flow, the inhomogenous wave equation in the frequency domain containing a source term $s(\boldsymbol{r}, f)$:

$$(\nabla^2 - k^2)p(\boldsymbol{r}, f) = s(\boldsymbol{r}, f) \tag{1}$$

In many practical situations the source $s(\boldsymbol{r}, f)$ is concentrated in a limited region of space embedded in a uniform medium. The acoustic field $p(\boldsymbol{r}, f)$ can formally be estimated for a given source distribution $s(\boldsymbol{r}, f)$ by means of Green's function. The solution obtained in this case is unique. The so-called inverse problem of determining $s(\boldsymbol{r}, f)$ from the measurement of $p(\boldsymbol{r}, f)$ outside the source region does not have a single solution without at least some additional information on the structure of the source. This statement can be demonstrated by considering another field of sound[17]: $p(\boldsymbol{r}, f) + \eta(\boldsymbol{r}, f)$, where $\eta(\boldsymbol{r}, f)$ is a smooth function vanishing outside the source region. The pressure field outside the source region is then exactly equal to the original one. However, the total field is now solution of

$$(\nabla^2 - k^2)[p(\boldsymbol{r}, f) + \eta(\boldsymbol{r}, f)] = s(\boldsymbol{r}, f) + (\nabla^2 - k^2)\eta(\boldsymbol{r}, f) \tag{2}$$

with a new source function. This result demonstrates that measuring the acoustic field outside the source region is not sufficient to determine the source on its own.[18] Furthermore, the Helmholtz operator acts as a low-pass filter in the wave-number domain, and details of $s(\boldsymbol{r}, f)$ on a scale smaller than the acoustic wavelength are lost. Consequently, the source function cannot be recovered, even using an infinite number of microphones. In summary, the concept of extended noise source measured through its radiation can only be viewed as an equivalence between source functions radiating the same pressure field.

B. Nature of the Estimation Problem—Choice of a Source Model

The conclusion at the end of the preceding section is essential to determine the nature of the problem we want to solve. In practical situations, it is not the details of the source functions that are needed but their directivity pattern in the far field. In the case where only one source region is considered, there is no need to perform a sophisticated process because a classical computation of spectrum gives the desired far-field information. The problem arises when different extended source regions radiate simultaneously, as the slats, the flaps, and the landing gears for an aircraft at landing (subregions for each main source domain may also be conveniently defined). The objective is to extract the directivity pattern of each region from the acoustic data. To proceed, it is necessary to model the source areas. Based on discussion in Sec. II.A, a distribution of monopoles, dipoles, or quadrupoles is suitable to achieve this modeling. In the following, we use monopole source distributions and insist on the fact that this choice is not based on any assumption about the structure of the actual sources. It has been chosen because this is the simplest equivalent model. Furthermore, a monopole source distribution does not mean that the directivity pattern is a priori isotropic: correlated monopoles with phase relationships can model any directivity pattern. So, a valuable equivalent source model could be a set of correlated monopoles. It is clear that the problem of finding both the amplitude of the sources and their correlation function in amplitude and phase involves a very large number of parameters. It is difficult to solve this problem at this level using a limited number of microphones. Fortunately, a majority of aerodynamic noise sources have smooth directivity patterns. This means that if the aperture angle of an array of microphones seen from the overall source region is not too large the directivity pattern of each region can be considered as isotropic within this aperture.

III. Array and Model CSM

The source power levels estimation is based on the CSM $[\Gamma^{mes}(f)]$ computed with the output signals of the array that contains all of the sound pressure levels (SPLs) of interest, associated with propagation operators, and on a modeling $[\Gamma^{mod}(f)]$ of this matrix. The description of these two matrices follows.

A. Measurement CSM

We consider an overall source domain $\mathcal{D}$ located in the (x_1, x_2) plane split into Q effective noise radiating areas D_q (Fig. 1). An array of M microphones located in front of $\mathcal{D}$ records the radiated pressure. We assume that the acoustic sources are random and stationary. Let $p_n^{mes}(t)$ be the pressure recorded by microphone n. The cross-correlation function $C_{m,n}^{mes}(\tau)$ between the microphone signals n and m is defined as

$$C_{m,n}^{mes}(\tau) = E\left[p_m^{mes}(t)\, p_n^{mes}(t+\tau)\right] \tag{3}$$

where $E[.]$ is the expectation operation.

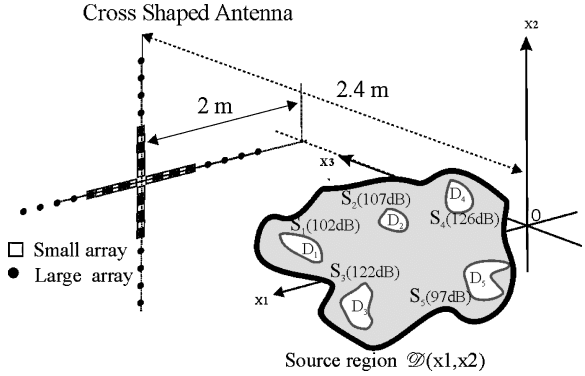

Fig. 1 Geometry of the source levels estimation problem.

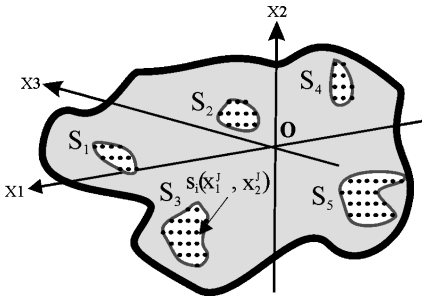

Fig. 2 Modeling of the source areas with sets of uncorrelated monopoles.

The cross-power spectral $\Gamma^{mes}_{m,n}(f)$ between $p^{mes}_m(t)$ and $p^{mes}_n(t)$ is the Fourier transform of $C^{mes}_{m,n}(\tau)$ (Wiener–Khintchine theorem):

$$\Gamma^{mes}_{m,n}(f) = \int_{-\infty}^{\infty} C^{mes}_{m,n}(\tau) e^{2\pi j f \tau}\, \mathrm{d}\tau \tag{4}$$

The measured array CSM of all signals $p^{mes}_m(t)$ $(m = 1, 2, \ldots, M)$ is defined by

$$[\Gamma^{mes}(f)] = \begin{bmatrix} \Gamma^{mes}_{1,1}(f) & \cdot & \Gamma^{mes}_{1,M}(f) \\ \cdot & \cdot & \cdot \\ \Gamma^{mes}_{M,1}(f) & \cdot & \Gamma^{mes}_{M,M}(f) \end{bmatrix} \tag{5}$$

B. Model CSM

According to the discussion in Sec. II.B, the acoustic source areas $D_q (q = 1, \ldots, Q)$ are each modeled with a set of N_q closely spaced (with respect to the acoustic wavelength) uncorrelated monopoles (Fig. 2). It follows that the total number of virtual sources used to characterize all of the source areas belonging to $\mathcal{D}$ is

$$J = \sum_{q=1}^{Q} N_q$$

With a source function $s_i(t)$ for each monopole, the correlation function between two monopoles is

$$C_{i,j}(\tau) = E[s_i(t) s_j(t+\tau)] = C_i(\tau)\delta_{i,j} \tag{6}$$

where δ_{jk} is the Kronecker delta.

The spectrum of $s_i(t)$ is $S_i(f)$, the Fourier transform of $C_i(\tau)$ [Eq. (6)]. The problem of the source power levels estimation is then to find the J parameters $S_i(f)$ of the model for each frequency. To proceed, it is necessary to define the general structure of the array CSM for uncorrelated monopole sources and then choose the J parameters $S_i(f)$ such that the model CSM fits at best the SPLs measured.

To compute the model CSM, we begin by expressing the pressure radiated on the array:

$$p^{mod}_n(t) = \sum_{i=1}^{J} \frac{s_i(t - R_{\mathrm{in}}/c)}{R_{\mathrm{in}}} \tag{7}$$

where R_{in} is the distance from the source i to microphone n. Replacing now $p^{mes}(t)$ by $p^{mod}(t)$ in Eq. (3) to obtain the modeled cross correlation:

$$C^{mod}_{m,n}(\tau) = E\left[p^{mod}_m(t) p^{mod}_n(t+\tau)\right] \tag{8}$$

one obtains from Eqs. (6) and (7) for $C^{mod}_{m,n}(\tau)$:

$$C^{mod}_{m,n}(\tau) = \sum_{i=1}^{J} \frac{C_i(\tau + (R_{\mathrm{im}} - R_{\mathrm{in}})/c)}{R_{\mathrm{im}} R_{\mathrm{in}}} \tag{9}$$

The Fourier transform of $C^{mod}_{m,n}(\tau)$ gives the model for the CSM:

$$\Gamma^{mod}_{m,n}(f) = \sum_{i=1}^{J} \frac{e^{jk(R_{\mathrm{im}} - R_{\mathrm{in}})}}{R_{\mathrm{im}} R_{\mathrm{in}}} S_i(f) \tag{10}$$

where $k = 2\pi f/c$ is the acoustic wave number.

For further developments $\Gamma^{mod}_{m,n}(f)$ is written in the following compact form:

$$\Gamma^{mod}_{m,n}(f) = \sum_{i=1}^{J} G_{m,i} S_i(f) G^*_{n,i} \tag{11}$$

with $G_{m,i} = e^{jkR_{\mathrm{im}}}/R_{\mathrm{im}}$.

IV. Least-Square Solutions for Source Power Levels Estimation

The first idea for finding $S_i(f)$ could simply be to solve for each frequency:

$$[\Gamma^{mes}(f)] = [\Gamma^{mod}(f)] \tag{12}$$

However, there is a serious limitation to the direct solution of Eq. (12) in obtaining the exact $S_i(f)$. The system of $M(M+1)/2$ independent equations resulting from the hermitian matrix can be underdetermined or overdetermined, depending on the value of the number J of unknowns. Because there is no exact solution, one tries to find approximations, that is, the mean square error between the two matrices[19]

$$F(S) = \sum_{m,n=1}^{M} \left| \Gamma^{mes}_{m,n} - \sum_{j=1}^{J} G_{m,j} S_j G^*_{n,j} \right|^2 \tag{13}$$

is as small as possible. Let us develop Eq. (13) in the following form:

$$F(S) = A - 2\sum_{i=1}^{J} U_i S_i + \sum_{i,j=1}^{J} S_i V_{i,j} S_j \tag{14}$$

with

$$A = \sum_{m,n=1}^{M} \left|\Gamma^{mes}_{m,n}\right|^2, \qquad U_i = \sum_{m,n=1}^{M} G_{m,i} \Gamma^{mes}_{m,n} G^*_{n,i}$$

$$\text{and} \qquad V_{i,j} = \left| \sum_{m=1}^{M} G_{m,i} G^*_{m,j} \right|^2$$

The condition for $F(S)$ to be a minimum is

$$\frac{\partial F(S)}{\partial S_i} = 0 \qquad \text{for} \qquad 1 \le i \le J \tag{15}$$

By solving the minimization problem, we arrive at the square linear system:

$$\sum_{j=1}^{J} V_{i,j} S_j = U_i \qquad \text{for} \qquad 1 \le i \le J \tag{16}$$

which can also be written in a matrix form as follows:

$$[V]\tilde{S} = \tilde{U} \tag{17}$$

with:

$$[V] = \begin{bmatrix} V_{1,1} & \cdot & V_{1,J} \\ \cdot & \cdot & \cdot \\ V_{J,1} & \cdot & V_{J,J} \end{bmatrix}, \qquad \tilde{S} = \begin{bmatrix} S_1 \\ S_J \end{bmatrix}, \qquad \tilde{U} = \begin{bmatrix} U_1 \\ U_J \end{bmatrix}$$

If $[V]^T[V]$ has an inverse, the vector solution $\tilde{S}$ of the normal equation is also a solution of the least-squares problem. However, it is well known that the solution of a linear system of the form of Eq. (17) based on the exact pseudoinverse results are poor solutions.[20–23] There have been many attempts at relaxing the equations. This can be achieved in direct methods by modifying or removing the small eigenvalues[21] in the matrix (i.e., $[V]^T[V]$ in the present application) of the normal equation or in the iterative case by stopping the iterations when the error attains a sufficiently small energy.[22] The relaxed methods have also been used with additional constraints on the data, and this solution has been successfully demonstrated.[24] Among the different constraints, the nonlinear positivity has been shown to be powerful and useful in overcoming the instability and nonuniqueness of the solution. It is then sensible to consider that a power spectrum has only positive values in order to obtain such regularized solutions. This leads to solve a new problem under nonlinear constraint and requires selecting an optimization method for nonlinear constraints. The choice is not very simple because many techniques compute a sequence of iterations that are not guaranteed to be feasible. Furthermore, these techniques are very costly in computation time because they attempt to satisfy the nonlinear constraint exactly at each iteration. In contrast, optimization methods for solving an unconstrained problem are efficient. This is why we define a new set of real unknowns $\alpha_i (1 \le i \le J)$ such that $S_i = \alpha_i^2$ to integrate implicitly the constraint in S_i. After this transformation, $F(\alpha)$ is a polynomial of fourth degree and its derivative a polynomial of third degree.

Now, at last two questions arise: on the existence of a unique global maximum (uniqueness of the solution) and on the choice of the initial guess to find a global maximum (and not a local one).

It is generally difficult to answer these questions theoretically when the estimation problem has nonlinearity characteristics such as the one that is under study in the paper. Today, we can only say that we have obtained different solutions and minima starting from very different values of the initial guess. However, it has been found in all of the simulations performed that the initial guess $\alpha_i^2 = U_i$ [Eq. (14)] leads to the global minimum, although we lack general proof for this observation.

The computation procedure consists first in sampling the source areas, then in determining the power levels α_j^2 of virtual uncorrelated monopoles located at each of the sampling points, by minimizing the error between the measured and model matrices:

$$F(\alpha) = \sum_{m,n=1}^{M} \left| \Gamma_{m,n}^{mes} - \sum_{j=1}^{J} G_{m,j} \alpha_j^2 G_{n,j}^{*} \right|^2 \tag{18}$$

Among all of the methods available to perform nonlinear optimization,[25] we chose an efficient and robust algorithm called the restarted conjugate gradient method to compute the α_j^2. This method is well documented from a statistical point of view[26] and from a numerical point of view.[27] An efficient well-debugged software version of the algorithm is available.[28]

After this step, the total power level output $P_{I,q}(f)$ of the source area D_q is obtained by summing the power levels α_j^2 of all monopole sources that are used in the modeling of D_q:

$$P_{I,q} = \sum_{j=1}^{N_q} \alpha_j^2 \tag{19}$$

We will call SEM this overall technique aiming at finding $P_{I,q}(f)$.

As mentioned in Sec. II.B, the result is valid only around the direction $\boldsymbol{u}$ and in the aperture $\Delta\boldsymbol{u}$ of the measuring array, seen from the source region. Consequently, in the acoustic far field, the SPL at a large distance R from the sources and around the direction $\boldsymbol{u}$ is modeled as

$$P(f, R\boldsymbol{u}) = \sum_{q=1}^{Q} \frac{P_{I,q}(f)}{R^2} \tag{20}$$

In conclusion, Eq. (20) can be considered as the mean directivity pattern of each radiating area q in the direction $\boldsymbol{u}$ averaged on $\Delta\boldsymbol{u}$. Then, rotating the measuring array around the global radiating region enables us to estimate the full directivity pattern $P(f, \boldsymbol{u})$.

V. Numerical Simulations

The objective of this section is twofold. In the first part we consider monodimensional configurations to compare the performances of the CBF method with those of the SEM. In the second part, we present some results obtained by the SEM involving two-dimensional configurations that are of practical interest.

A. Comparison of the CBF and SEM Performances

For the three tests considered here, the sources are monopoles placed on a line 2 m in length, located at a distance $D = 2$ m from the array composed of 15 microphones equally spaced every 0.1 m. The length of the array is $L = 1.4$ m (Fig. 3).

1. Two Sources Spaced at More than 3 dB Beam Width

The source S_1 is located at $x = -0.2$ m with an amplitude of 70 dB, and S_2 is located at $x = +0.2$ m with an amplitude of 65 dB (Fig. 4). S_1 and S_2 are separated from each other by more than a standard beam width $\Delta X_{3\text{dB}} = 1.3\lambda$ ($\lambda = c/f$; with $c = 340$ m/s and $f = 3$ kHz). The CBF result method exhibits two main peaks (Fig. 4) with a width of 3λ. Their locations and amplitudes coincide

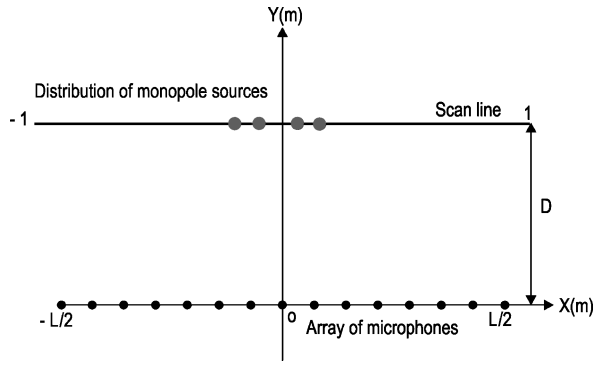

Fig. 3 Geometry of the numerical simulation used to compare the resolution between the CBF method and the SEM.

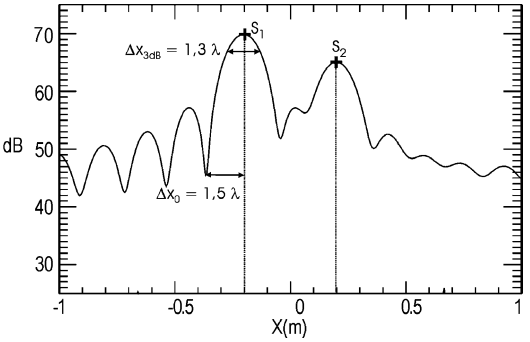

Fig. 4 Scenario of two uncorrelated monopoles S_1(70 dB) and S_2(65 dB) spaced by more than one 3-dB bandwidth—result provided by the CBF method.

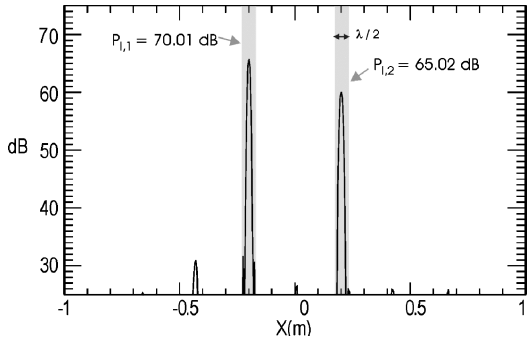

Fig. 5 Results obtained by the SEM for the simulation presented in Fig. 4.

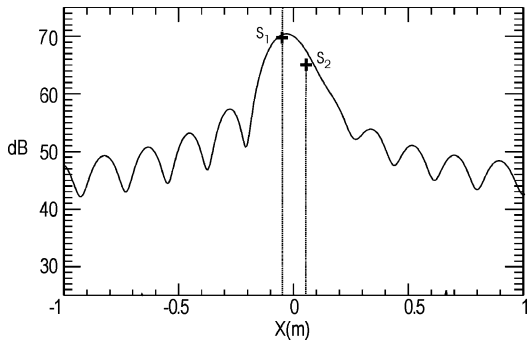

Fig. 6 Scenario of two uncorrelated monopoles S_1(70 dB) and S_2(65 dB) spaced by less than 3-dB bandwidth—result obtained by the CBF method.

with those of the actual sources S_1 and S_2. Figure 5 shows the power levels (i.e., 20 log α_j) of monopoles, distributed over the scan line, computed with the parametric method. It is obvious here that the spatial resolution of the new method is much better than that of the CBF because the width of two peaks at the location of S_1 and S_2 is only of $\lambda/2$. However, contrary to the CBF, the amplitudes of the two sources do not result from the maxima of the peaks. With the SEM, an integration over $\lambda/2$ the spatial extent of the two peaks is needed to find the power levels of the sources. Accordingly, the amplitudes of S_1 and S_2 are respectively provided with a good degree of accuracy by $P_{I,1} = 70.01$ dB and $P_{I,2} = 65.02$ dB [Eq. (19)].

2. Two Sources Spaced by Less than 3 dB Beam Width

The parameters of the simulation are the same as those used earlier, except that here S_1 is located at $x = -0.05$ m and S_2 at $x = +0.05$ m (Fig. 6). As predicted, the CBF fails to resolve the two sources that do not respect the 3-dB bandwidth criterion (Fig. 6). However, the result exhibits a power level of 70.5 dB at the location of S_1 (instead of 70 dB expected) and 67 dB at the location of S_2 (instead of 65 dB). The source locations are correctly found with the parametric method (Fig. 7). Furthermore, the integrated power levels $P_{I,1} = 70.07$ dB and $P_{I,2} = 64.72$ dB over the spatial extent of the two peaks correspond respectively to the actual power levels of S_1 and S_2.

3. Two Source Distributions

The third case concerns two source distributions Ω_1 and Ω_2 at 2 kHz, spaced by 0.15 m. They are each composed of seven uncorrelated monopoles spaced every 0.05 m (Fig. 8). The total power level output of Ω_1 is 63.45 dB, and it is of 78.45 dB for Ω_2. The present configuration is not favorable for the CBF: Ω_1 and Ω_2 are not resolved, and their amplitudes cannot be deduced from the result (Fig. 8). The situation is completely different with the SEM because Ω_1 and Ω_2 are separated, and their total power level outputs computed over the spatial extent shown in grey (Fig. 9) are in agreement with the expected ones.

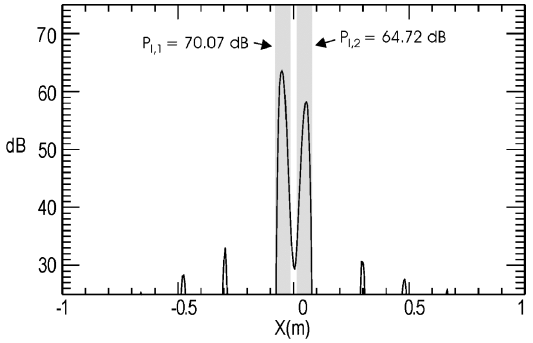

Fig. 7 Result provided by the SEM for the numerical simulation presented in Fig. 6.

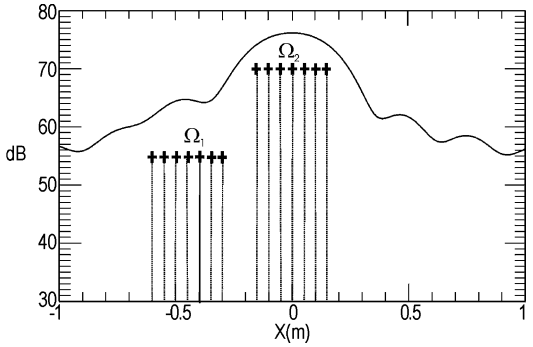

Fig. 8 Two source distributions composed each of seven uncorrelated monopoles spaced by less than 3-dB bandwidth—result obtained with the CBF method.

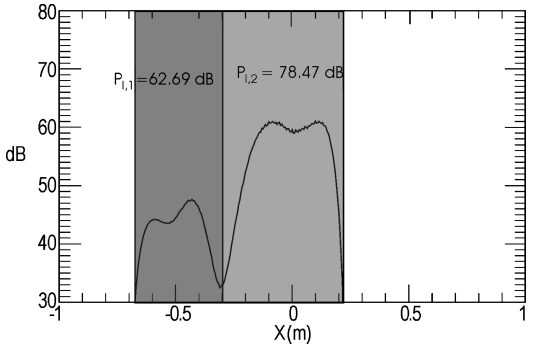

Fig. 9 Result obtained with the SEM for the simulation presented in Fig. 8.

B. Accuracy of SEM in Two-Dimensional Simulations

The example presented in this section illustrates the many possibilities of the SEM in the power level estimation of two-dimensional sources similar to those encountered in practical situations. The array used for the simulations has the same design as the one in the experiment performed with the aircraft model (Sec. VI). It is composed of two sub-cross-shaped arrays with microphones periodically spaced along their two arms (Fig. 1). The large array works in a low-frequency range with a 10-cm distance between two microphones. The small array works in a high-frequency range with a 5-cm separation distance.

1. Six Source Areas Including Two Monopole Sources

The geometry of the simulation shows the locations of six source areas at 7324 Hz and between the brackets their total power level output (Fig. 10). Figure 11 shows the six source areas evenly sampled every 0.04 m and the integrated power levels found by using the SEM. The result is in agreement with Fig. 10. The power levels of the monopole sources used to model each source area in Fig. 10 are presented in Fig. 12 under the form of a localization map. As for the monodimensional cases (see Sec. V.A), the high-resolution

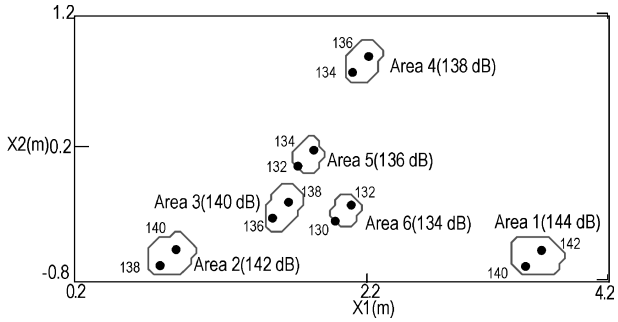

Fig. 10 Scenario 1: six source areas including two monopole sources.

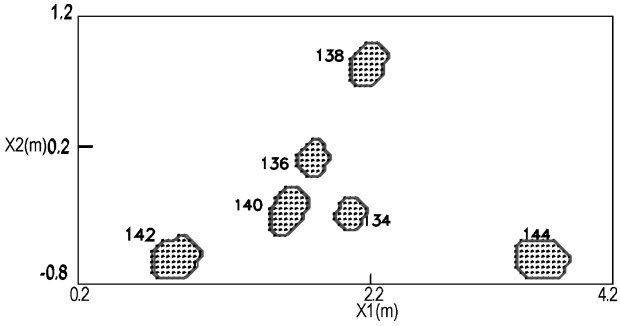

Fig. 11 Spatial sampling of the source regions considered in Fig. 10 and their integrated power levels (SEM result).

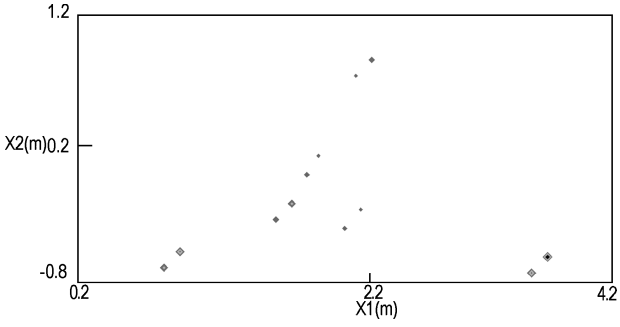

Fig. 12 Location map obtained with the parametric method for the simulation shown in Fig. 10.

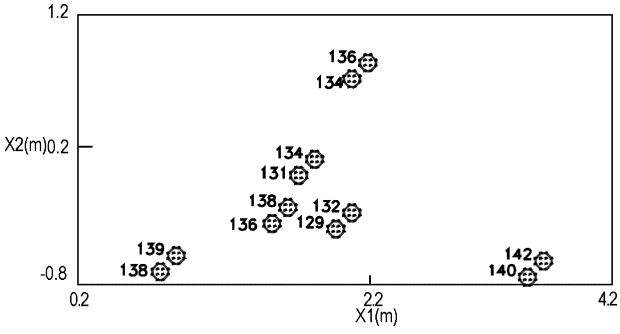

Fig. 13 Levels of the monopole sources considered in Fig. 10 obtained by integrating the power levels over each of the small regions shown here.

capabilities of the parametric method are again demonstrated because only the monopole sources considered for the simulation are dominant. Furthermore, the integrated power levels over the small areas shown in Fig. 13 are in agreement, within 1 dB, with those of each of the monopoles presented in Fig. 10.

2. Nine Source Areas Including up to Four Monopole Sources

The configuration considered here is more complex that in the preceding example because the number of monopoles at 11,719 Hz is more important in the source areas (Fig. 14). In Fig. 15 we show

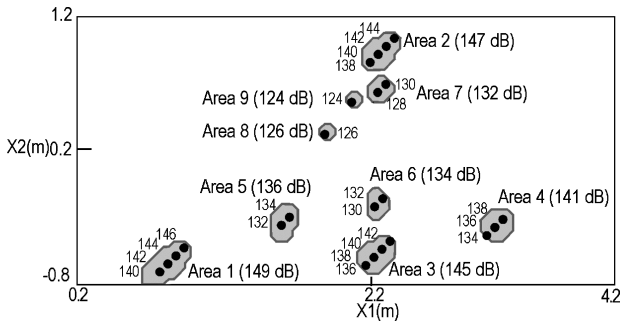

Fig. 14 Scenario 2: Nine source areas including one to four monopole sources.

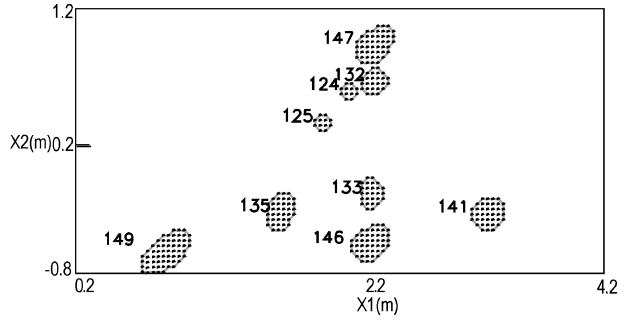

Fig. 15 Spatial sampling of the areas displayed in Fig. 14 and their integrated power levels.

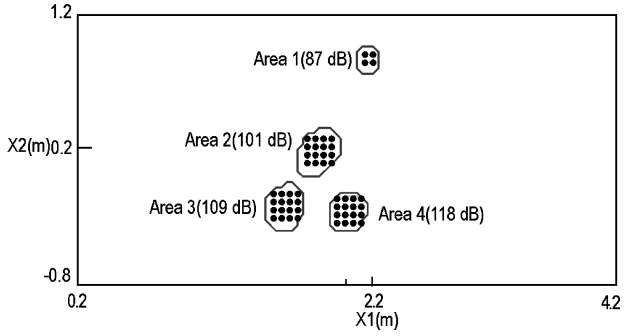

Fig. 16 Scenario 3: four source areas including four to 16 monopole sources.

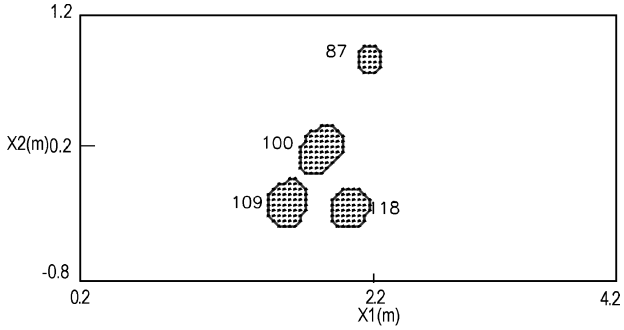

Fig. 17 Spatial sampling of the source regions shown in Fig. 16 and their integrated power levels.

the computational grids and the integrated power levels. It appears that the results correspond to the expected power levels presented in Fig. 14.

3. For Source Areas Including up to 16 Monopole Sources

In this last case, the monopole sources at the frequency of 2808 Hz nearly cover the whole of each source area (Fig. 16). The result in Fig. 17 demonstrates again the good accuracy of the SEM in more realistic simulation of extended sources.

VI. Experimental Results

Two sets of results are presented. In the first set one performs the experimental validation of the SEM. The second set presents an analysis of the data.

A. Experimental Setup and Data Processing

The experiments described in this study have been performed with a model of an A320/A321 aircraft of Airbus Industry in the CEPRA 19 anechoic wind tunnel[9,10] (Fig. 18). The aim of this experiment was to characterize the airframe noise and in particular to quantify the contribution to the acoustic far field of the main landing gear (MLG), the nose landing gear (NLG), and the high-lift devices. The main parameters of the experiments are the deflection angles slat (SL) and flap (FL) of the slats and of the flaps, the pitch angle I of the model, and the wind-tunnel flow velocity V ranging from 30 up to 60 m/s. The noise radiated by the model is measured using a cross-shaped array, equipped with 40 half-inch microphones AKSUD 3211. The microphones are distributed along the two arms of the array in the same way as described in Sec. V.B. Because the antenna is located outside the flow, convection and refraction effects occur between the sources on the aircraft model and the locations of the microphones. They are taken into account by applying flow corrections on the propagation time,[29,30] which are used in the computation of the model array CSM. The virtual monopoles of the source modeling extend on the wing surface and belong to a grid sampled every $\Delta x_1 = 0.04$ m, $\Delta x_2 = 0.04$ m. $[\Gamma^{mes}]$ is estimated using 200 data blocks including 1024 samples each at the sampling frequency f_s. All of the SPLs are computed up to $f_{\max} = f_s/2$. They are plotted vs normalized frequencies $f/f_{\max}$ in the range [0, 1]. The results presented in this chapter have been obtained with the procedures implanted on a workstation to compute either the SEM or the CBF for configurations tested in the CEPRA 19 anechoic wind tunnel. The details of these procedures are not given here to keep a reasonable length to the paper.

B. Validation

1. Direct Validation

We consider the case where FL = 25 deg, SL = 0 deg, MLG = UP, NLG = UP. This configuration generates acoustic sources extended over the complete wing. In a first step, we examine the power level radiated by the wing (Fig. 19) in the far field. Figure 19 also displays the computational domain, which is surrounded with a grey line.

The wing acoustic far field estimated using the SEM (dashed line) is compared in Fig. 20 to the experimental spectrum (solid line) provided by Microphone 18 on the array (Fig. 18). The spectra exhibit the same characteristics: a narrowband phenomenon at low frequencies, a constant level at medium frequencies, and finally a decrease in the high-frequency domain. The computed and measured SPLs nearly coincide, the difference remaining within 1 dB. Furthermore, as expected, the noise source areas of the aircraft model other than the wing sources weakly contribute to noise levels in the far field. The good accuracy of the results obtained by using the data of the microphone 18 has also been observed for the other microphones of the antenna during the validation tests. This can be explained by the fact that the majority of aerodynamic noise sources have smooth directivity patterns, which are correctly measured within the spatial aperture of the antenna.

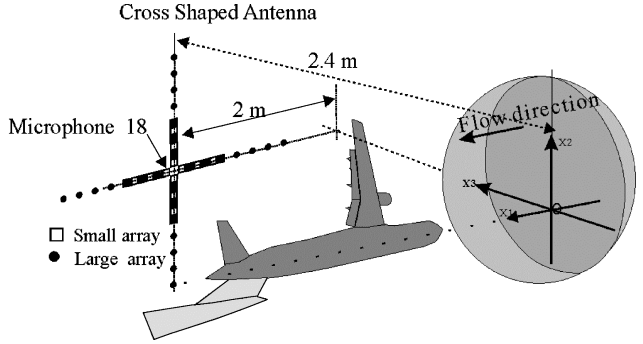

Fig. 18 Experimental setup. A model of an A320/A321 aircraft of Airbus Industry in the CEPRA 19 anechoic wind tunnel. The cross-shaped array is composed of 40 microphones.

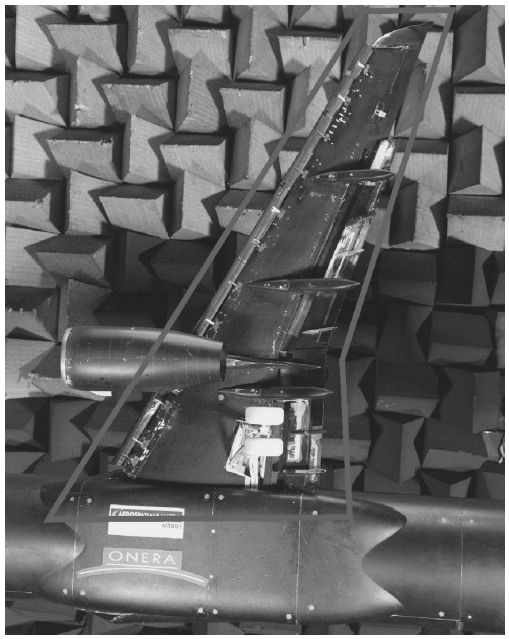

Fig. 19 Detailed view of the complete wing.

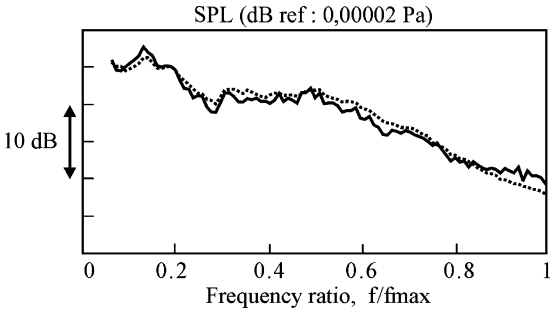

Fig. 20 Comparison between spectra computed with the SEM (- - - -) and measured in the far field by microphone 18 (——) for the complete wing.

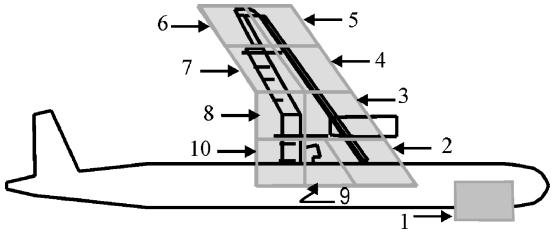

Fig. 21 Main source areas used to apply the SEM.

2. Cross Validation

In the research conducted on airframe noise by ONERA, a CBF technique suitable for a cross-shaped array has been developed and applied to localize the acoustic sources on an A320/A321 aircraft model. Ten main source regions have been identified from the localization results, and they are presented in Fig. 21.

In this example, the main sources are tone noise sources that are found on the trailing edge of the flap. Attention is focused here on area number 10, located near the junction of the inboard flap with the fuselage, where beam forming shows the presence of a main acoustic source (the darkest regions are the dominant sources

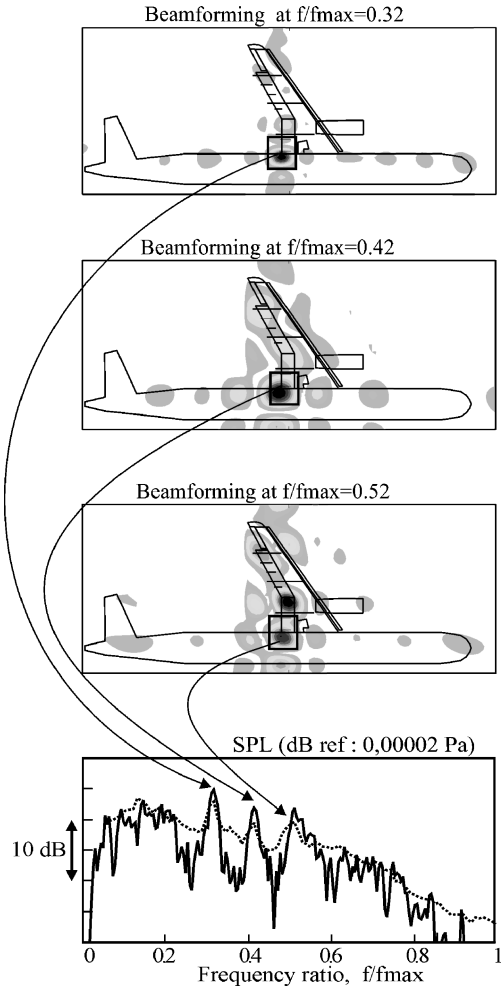

Fig. 22 Beam forming for three frequencies. Comparison between the spectra of the inner part of the flaps obtained from the SEM data (- - - -) and by the TSM (——).

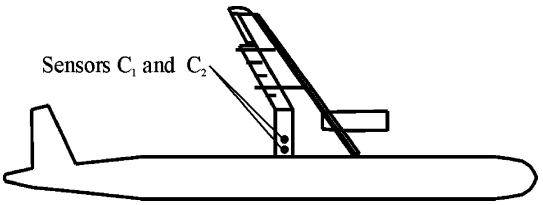

Fig. 23 Location of the two pressure sensors.

and the clearest regions the weak sources) in different frequency bands (Fig. 22). Although the computation with the SEM is achieved without difficulty, the accuracy of the result cannot be checked as in the preceding example by using single microphone data. It is obvious that a microphone is not only receptive to the noise radiated by source area 10, but measures the global noise generated by the aircraft model. Fortunately, the model was equipped with pressure sensors in this region (Fig. 23). The result of the SEM can thus be compared with data obtained using the so-called three-sensors method[9] (TSM), based on a completely different signal processing (see Appendix).

This technique allows us to extract the spectrum corresponding to a source area measured locally by two sensors C_1 and C_2 from the spectrum of a microphone placed in the far field. In Fig. 22, we show spectra provided by the SEM (dashed line) and by the TSM (solid line). The result exhibits a narrowband noise in the low normalized frequency range from 0.038 to 0.22. Tones also appear at the frequencies of 0.32, 0.42, and 0.52, and, as in the preceding example, the spectra decrease in the high-frequency domain. The

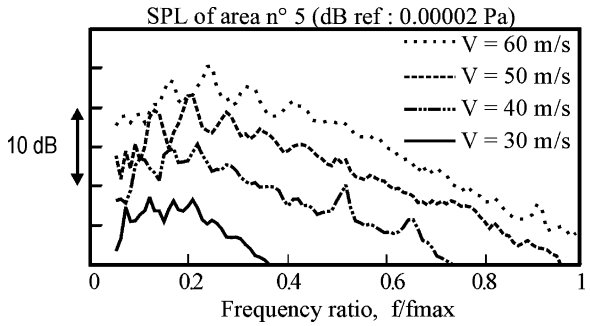

Fig. 24 Influence of flow velocity on the noise radiated by the area number 5 in a landing configuration.

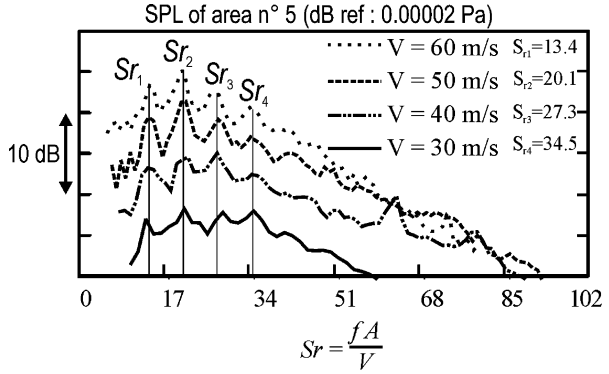

Fig. 25 Normalized spectra presented Fig. 24 as a function of the Strouhal number *Sr*.

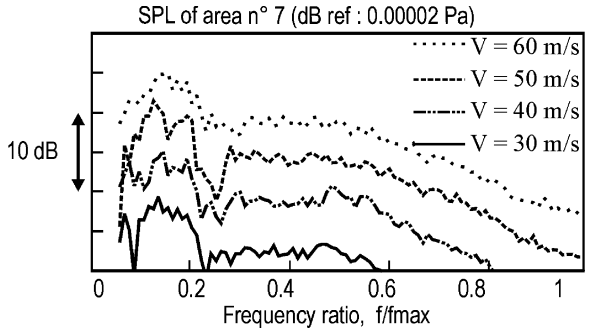

Fig. 26 Influence of flow velocity on the noise radiated by the area number 7 in a landing configuration.

fairly good agreement between the two spectra, especially around the peaks, provides a cross validation of the SEM by using the TSM.

C. Data Analysis

Once SEM is experimentally validated, it provides a large database, which can be used to identify the characteristics of each physical mechanism governing noise radiation in the far field. Attention is focused here on the source areas 5 and 7, defined on the model wing (Fig. 21), for a landing configuration (FL = 25 deg, SL = 27 deg, $I = 6$ deg, MLG = UP, NLG = UP) and four wind-tunnel velocities, namely, $V = 30$, 40, 50, and 60 m/s.

Figure 24 shows the spectra of area 5 located at the outboard slat for the four velocities. It appears first that the peak frequency seems to increase linearly with the velocity. This suggests we should normalize the frequency using a Strouhal number $Sr = fA/V$, where A is a typical length (Fig. 25). Now the peaks of the four curves are periodically spaced (every $7x$ Sr) for $13 < Sr < 43$ because their origin is not yet known. It has not been possible to find a simple relationship between the levels and the flow velocity.

The characteristics of the noise radiated by area 7 located at the outboard flap are very different. The spectra presented in Fig. 26 show that the noise level in decibels increases proportionally to the

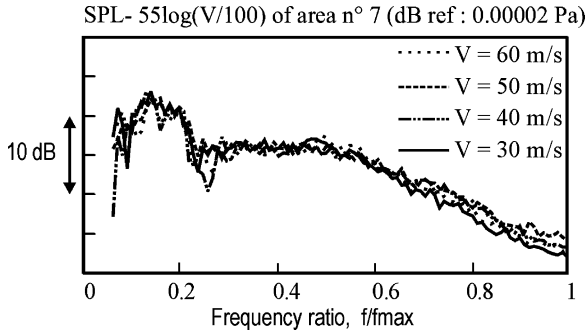

Fig. 27 Same legend as in Fig. 26, but here the amplitudes of the spectra are normalized by a factor following a speed law in $V^{5.5}$.

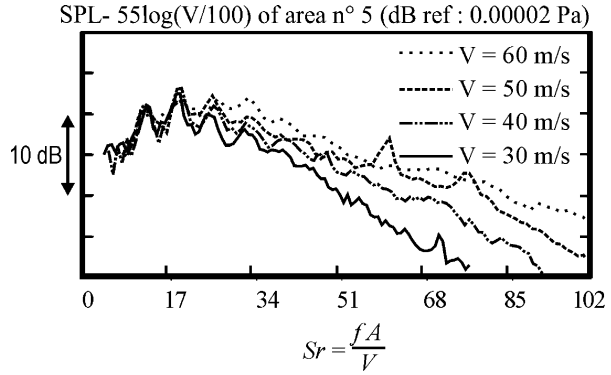

Fig. 28 Same legend as in Fig. 25, but here the amplitudes of the spectra are normalized by a factor following a speed law in $V^{5.5}$.

logarithm of the flow speed. Moreover, the shapes of the spectra are nearly identical for all of the velocities, showing that the mechanism is not Strouhal dependent. This can be clearly seen in Fig. 27, where all of the spectra are normalized by a factor following a speed law in $V^{5.5}$. The same normalization operation is applied in Fig. 28 with the spectra of area 5 presented in Fig. 25. Clearly, one observes that the speed law $V^{5.5}$ is only valid in low frequencies ($f < 0.25$). Otherwise, the disagreement between the spectra increases with the frequency.

VII. Summary

The estimation problem for the power levels of extended acoustic sources has been examined, and a parametric method to solve this problem has been described. This method is based on the direct use of the array CSM and its modeling.

This approach has allowed us to build a SEM method with high-resolution capabilities. Thus, the beam patterns of the source distributions are not corrupted by the array response, which is the principal limitation of the CBF. With this intrinsic quality of the SEM, the absolute levels of the extended sources can be directly obtained by adding the contributions of the monopole sources computed with the parametric method to model the extended sources. The spatial resolution capabilities have been illustrated by comparing the beam patterns computed using the beam forming, and the parametric method in numerical simulations where the characterization of several types of monopole source distributions have been considered. Furthermore, the SEM has been applied to experiment data measured during tests conducted with a 1/11th-scaled Airbus A320/A321 aircraft model in the CEPRA 19 anechoic wind tunnel.

The results obtained from numerical simulations and from application to experimental data show that the estimation method is a valuable tool for obtaining the power levels of multiple source areas in practical situations of interest.

The SEM will be used in a near future to carry out a quantitative study of airframe noise from experiments carried out in the French anechoic wind tunnel CEPRA 19 and the German Netherlands wind tunnel DNW with an aircraft model of Airbus.

Appendix: Three-Sensors Method

Consider a random stationary acoustic source $s(t)$ and its Fourier transform $S(f)$ in a time interval T. Its SPL can be defined as $S(f) = \langle |S(f)|^2 \rangle$. Two sensors C_1 and C_2 are located in the vicinity of the source, and it is assumed that their outputs are linearly related to $s(t)$. Also, a microphone M records the pressure in the far field at distance R. The model is the following:

$$C_1(f) = H_1(f)s(f) + N_1(f), \qquad C_2(f) = H_2(f)s(f) + N_2(f)$$
$$P_M(f) = s(f)e^{-ikR}/R + N_3(f)$$

where $H_1(f)$ and $H_2(f)$are unknown linear transfer functions and $N_i(f)$ $(i = 1, 2, 3)$ the contribution of all of the other sources. We assume that these three contributions are uncorrelated. Under this assumption, TSM consists in extracting $S(f)$ from the three cross spectra:

$$S(f) = R^2 \frac{\Gamma_{c_1,M}(f)\Gamma_{M,c_2}(f)}{\Gamma_{c_1,c_2}(f)}$$

with

$$\Gamma_{c_1,c_2}(f) = \langle C_1(f)C_2^*(f) \rangle, \qquad \Gamma_{c_1,M}(f) = \langle C_1(f)P_M^*(f) \rangle$$
$$\Gamma_{M,c_2}(f) = \langle P_M(f)C_2^*(f) \rangle$$

Acknowledgments

The authors of this paper are grateful to M. Jean-Luc Akian, Jean Prieur, and Alain Julienne for many stimulating discussions. The result of the three-sensors method presented in Fig. 10 have been obtained by M. Renaud Davy. The Department of Computational Fluid Dynamics and Aeroacoustics of ONERA has supported the research described in this paper. The experiment with the aircraft model was performed under a contract from Airbus Industrie and SPAé (French Service of Aeronautic Programs).

References

[1]Kendall, J. M., "Airframe Noise Measurement by Acoustic Imaging," AIAA Paper 77-55, Jan. 1977.

[2]Grosche, F. R., Stiewitt, H., and Binder, B., "Wind-Tunnel Measurements with a Highly Directional Microphone," *AIAA Journal*, Vol. 15, No. 11, 1977, pp. 1590–1596.

[3]Élias, G., and Malarmey, C., "Utilisation d'Antennes Focalisèes pour la Localisation de Sources Acoustiques," *Proceedings of the 11th ICA Conference*, Paris, 1983, pp. 163–166.

[4]Élias, G., "Source Localisation with a Two-Dimensional Focused Array-Optimal Processing for a Cross-Shaped Array," Inter-Noise 95, Newport Beach, CA, 10–12 July 1995.

[5]Piet, J. F., and Élias, G., "Airframe Noise Source Localization Using a Microphone Array," AIAA Paper 97-1643, May 1997.

[6]Blacodon, D., Caplot, M., and Élias, G., "Source Localization Technique for Multiple Impulsive Sources," *Journal of Aircraft*, Vol. 26. No. 2, 1989, pp. 154–156.

[7]Humphreys, W. M., Brooks, T. F., Hunter, W. W., and Meadows, K. R., "Design and Use of Microphone Directional Arrays for Aeroacoustic Measurements," AIAA Paper 98-0471, Jan. 1998.

[8]Mosher, M., "Phased Arrays for Aeroacoustic Testing: Theoretical Development," AIAA Paper 96-1723, May 1996.

[9]Davy, D., and Remy, H., "Airframe Noise Characteristics of a 1/11 Model Airbus," AIAA Paper 98-2335, June 1998.

[10]Davy, R., Moens, F., and Rémy, H., "Aeroacoustic Behavior of a 1/11 Scale Airbus Model in the Open Anechoic Wind Tunnel Cepra 19," AIAA Paper-2002-2412, June 2002.

[11]Brooks, T. F., and Humphreys, W. M., "Effect of Directional Array Size on the Measurement of Airframe Noise Components," AIAA Paper 99-1958, May 1999.

[12]Katsaggelelos, A. K., "A Class of Iterative Signal Restoration Algorithms," *IEEE Transactions on Acoustics, Speech, and Signal Processing*, Vol. 38, No. 5, May 1990, pp. 778–786.

[13]Trussel, H. J., "The Feasible Solution in Signal Restoration," *IEEE Transactions on Acoustics and Signal Processing*, Vol. ASSP-32, No. 2, April 1984, pp. 201–212.

[14]Viberg, M., and Ottersten, B., "Sensor Array Processing Based on Subspace Fitting," *IEEE Transactions on Signal Processing*,Vol. 39, No. 5, May 1991, pp. 1110–1120.

[15]Schafer, R. W., Mersereau, R. M., and Richard, M. A., "Constrained Iterative Restoration Algorithms," *Proceedings of IEEE*, Vol. 69, No. 4, April 1981, pp. 432–450.

[16]Levy, A. J., "A Fast Quadratic Programming Algorithm for Positive Signal Restoration," *IEEE Transactions on Acoustics, Speech, and Signal Processing*, Vol. ASSP-32, No. 2, 1984, pp. 432–450.

[17]Ffowcs Williams, J. E., "Hydrodynamic Noise," *Annual Review of Fluid Mechanics*, Vol. 1, 1969, pp. 197–222.

[18]Dowling, A. P., and Ffowcs Williams, J. E., *Sound and Sources of Sound*, Ellis Horwood, Chichester, England, UK, 1983.

[19]Zoppellari, E., and Juvé, D., "Reduction of Hot Supersonic Jet Noise by Water Injection," AIAA Paper 98-2204, June 1998.

[20]Hunt, B. R., "Application of Constrained Least Squares Estimation to Image Restoration by Computer," *IEEE Transactions on Computing*, Vol. C-22, 1973, pp. 805–812.

[21]Shim, Y. S., and Cho, Z. H., "SVD Pseudoinverse Image Reconstruction," *IEEE Transactions on Acoustics, Speech, Signal Processing*, Vol. ASSP-29, Aug. 1981, pp. 904–909.

[22]Trussell, H. J., "Convergence Criteria for Iterative Restoration Methods," *IEEE Transactions on Acoustics, Speech, Signal Processing*, Vol. ASSP-31, Feb. 1983, pp. 129–136.

[23]Dougherty, R. P., and Stoker, R. W., "Sidelobe Suppression for Phased Array Aeroacoustic Measurements," AIAA Paper 98-2242, June 1998.

[24]Trussell, H. J., and Civanlar, M. R., "The Feasible Solution in Signal Restoration," *IEEE Transactions on Acoustics, Speech, Signal Processing*, Vol. ASSP-32, No. 2, April 1984, pp. 201–212.

[25]Gill, P. E., Murray, W., and Wright, M. H., *Practical Optimization*, Academic Press, London, 1981, pp. 59–66.

[26]Bard, Y., *Nonlinear Parameter Estimation*, Academic Press, New York, 1974.

[27]Bandler, J. W., "Computed-Aided Circuit Optimization," *Modern Filter Theory and Design*, edited by G. C. Temes and S. K. Mitra, Wiley, New York, 1973.

[28]Shanno, D. F., and Phua, K. H., "Minimization of Unconstrained Multivariate Functions," *ACM Transactions on Mathematical Software*, Vol. 6, Dec. 1980, pp. 618–622.

[29]Candel, S., Guédel, A., and Julienne, A., "Radiation, Refraction and Scattering on Waves in a Shear Flow," AIAA Paper- 76-544, July 1976.

[30]Amiet, R. K., "Refraction of Sound by a Shear Layer," *Journal of Sound and Vibration*, Vol. 58, No. 3, 1978, pp. 467–482.